Molecular Genetics and Metabolism Reports 33 (2022) 100932

Contents lists available at ScienceDirect

Molecular Genetics and Metabolism Reports

journal homepage: www.elsevier.com/locate/ymgmr

ITCH deficiency clinical phenotype expansion and mitochondrial dysfunction

Rachel Wolfe [a,b,1], Paige Heiman [a,1], Olivia D'Annibale [a,c], Anuradha Karunanidhi [a], Alyssa Powers [a,c], Marianne Mcguire [d], Bianca Seminotti [a], Steven F. Dobrowolski [e], Miguel Reyes-Múgica [e], Kathryn S. Torok [f], Al-Walid Mohsen [a,c], Jerry Vockley [a,c], Lina Ghaloul-Gonzalez [a,c,*]

[a] Division of Genetic and Genomic Medicine, Department of Pediatrics, University of Pittsburgh, Pittsburgh, PA, USA
[b] University of Pittsburgh, School of Medicine, University of Pittsburgh, Pittsburgh, PA, USA
[c] Department of Human Genetics, Graduate School of Public Health, University of Pittsburgh, Pittsburgh, PA, USA
[d] UPMC Clinical Genomics Laboratory, UPMC Magee-Womens Hospital, Pittsburgh, PA, USA
[e] Division of Clinical Chemistry, Department of Pathology, University of Pittsburgh, Pittsburgh, PA, USA
[f] Division of Rheumatology, Department of Pediatrics, University of Pittsburgh, Pittsburgh, PA, USA

ARTICLE INFO

Keywords:
ITCH
Autoimmune disease
Ubiquitination
Apoptosis
E3 ligase
Mitochondrial dysfunction

ABSTRACT

Autoimmune Disease, Multisystem, with Facial Dysmorphism (ADMFD) is an autosomal recessive disorder due to pathogenic variants in the *ITCH* gene. It is characterized by failure to thrive, dysmorphic facial features, developmental delay, and systemic autoimmunity that can manifest variably with autoimmune hepatitis, thyroiditis, and enteropathy, among other organ manifestations. It was originally described in 10 consanguineous Old Order Amish patients, and more recently in two patients of White British and Black German ethnicities. While the role of ITCH protein in apoptosis and inflammation has previously been characterized, a defect in cellular bioenergetics has not yet been reported in ITCH deficiency. Here we present a Caucasian female originally evaluated for possible mitochondrial respiratory chain deficiency, who ultimately was found to have two novel variants in *ITCH* with absence of ITCH protein in patient derived fibroblasts. Clinical studies of patient muscle showed mitochondrial DNA copy number of 57% compared to controls. Functional studies in skin fibroblasts revealed decreased activity of mitochondrial fatty acid oxidation and oxidative phosphorylation, and decreased overall ATP production. Our findings confirm mitochondrial energy dysfunction in a patient with ITCH deficiency offering the opportunity to assess alternative therapeutic options.

1. Introduction

Protein ubiquitination is an essential post-translational modification that plays a central role in protein recycling in eukaryotic cells [1,2]. ITCH (Itchy E3 Ubiquitin Protein Ligase), encoded by the *ITCH* gene, is a HECT E3 ubiquitin ligase important in regulation of the immune response and autoinflammation.

The *ITCH* gene was first identified in 1995 in a study using radiation to induce mutations in the Agouti locus in mice [3]. One of the homozygous mutations, named allele a^{18H}, caused chronic dermatitis and pruritus in the mutant animals. $Itch^{a18H/a18H}$ mice (mice with global loss of *Itch*) also were found to have splenomegaly, lymphadenopathy, skin

Abbreviations: UPS, Ubiquitin proteasome system; IF, Immunofluorescence analysis; FAO, Fatty acid oxidation; OXPHOS, Oxidative Phosphorylation; OCR, Oxygen consumption rate; IBD, Inflammatory Bowel Disease; TXNIP, Thioredoxin Interacting Protein; Tregs, T regulatory cells; TFP, Trifunctional protein; VLCAD, Very long-chain acyl-CoA dehydrogenase protein; DMEM, Dulbecco's Modified Eagle Medium; HECT, Homologous to the E6-Associated Protein C-Terminus; NOTCH1, Notch receptor 1 protein; FOXP3, Forkhead box P3 protein; TAX1BP1, TAX1-binding protein 1; MAVS, Mitochondrial antiviral signaling protein; ETC, Mitochondrial electron transport chain.

* Corresponding author at: Division of Genetic and Genomic Medicine, Department of Pediatrics, UPMC Children's Hospital of Pittsburgh, Rangos Research Building, Pittsburgh, PA 15224, USA.
E-mail address: lina.gonzalez@chp.edu (L. Ghaloul-Gonzalez).
[1] These first authors contributed equally.

https://doi.org/10.1016/j.ymgmr.2022.100932
Received 24 September 2022; Received in revised form 20 October 2022; Accepted 22 October 2022

inflammation, and lung mononuclear cell infiltration [4,5]. Subsequently, *Itch*$^{a18H/a18H}$ mice were shown to have lymphocyte proliferation in immune organs and architectural changes in the small intestine, similar to alterations seen in autoimmune pathologies like inflammatory bowel disease (IBD) [6].

In addition to immune regulation, ITCH has also been shown to ubiquitinate a variety of proteins involved in apoptosis and inflammatory signaling. Specifically, ITCH mediates polyubiquitination of thioredoxin interacting protein (TXNIP), an inhibitor of thioredoxin that interferes with its antioxidant properties [7–9]. ITCH leads to polyubiquitination of TXNIP and its proteasomal degradation, thereby increasing the thioredoxin levels, which in turn decreases reactive oxygen species (ROS) and prevents cellular apoptosis. By contrast, low levels of ITCH allow for inhibition of thioredoxin and increased apoptosis. Additional studies have shown that ITCH degrades tBid and p63, other proteins that regulate apoptosis through different pathways [10,11].

ITCH deficiency (Multisystem autoimmune disease with facial dysmorphism; MIM # 613385) was first described in humans in ten Old Order Amish children, all with the same truncating homozygous mutation, a frameshift in *ITCH* with a single base pair insertion in exon 6 (c.394dupA; p.Ile132Asnfs*9) (GenBank: NM_031483.7) [12]. Patients presented with organomegaly, failure to thrive, dysmorphic facial features, macrocephaly, developmental delay, gross motor and cognitive skills delay, and inflammatory cell infiltrate in the lungs, liver, and gut.

Nearly 10 years after the initial report, three additional patients with ITCH variants were described [13]. The first patient was a one-year-old Black German female from a consanguineous family with syndromic facial features, muscular dystrophy, short stature, psychomotor retardation, and muscular hypotonia. She experienced acute liver failure due to autoimmune hepatitis and ultimately required liver transplantation. She was found to have a homozygous splice variant in *ITCH*, c.1570-1G > A (GenBank: NM_031483.7) resulting in skipping of exon 18 and leading to aberrant mRNA processing. A second report described a 23-year-old non-consanguineous White British female with biallelic truncating variants in *ITCH* (GenBank: NM_031483.7) (c.603delA; p.Leu202Serfs*63) and (c.2005_2008delGAAA; p.Glu669Phefs*2) [14]. She was dysmorphic with camptodactyly of the fingers, and had severe chronic lung disease resembling asthma. The third report described a 16 year-old patient with biallelic splice site and truncating variants in *ITCH* (GenBank: NM_001257137) (c.337+2T>C) and (c.772C>T; p.Arg258*) who underwent hematopoietic cell transplantation with 2 years follow up post-transplantion [15]. She was dysmorphic with a severe phenotype including growth failure, developmental delay, macrocephaly, polyarthritis, enteropathy, lung disease and psoriasis, A comparison in phenotype of all previously reported patients including the one in this study is presented in Table 1.

Little is known about the relationship between ITCH and mitochondrial function. A link between mitochondrial physiology and the ubiquitin proteasome system (UPS) has been postulated, with mutations in intramitochondrial E3 ubiquitin ligase (*FBXL4*) leading to mitochondrial encephalopathy accompanied by severe deficiencies in mitochondrial bioenergetics and alterations in oxidative phosphorylation (OXPHOS) proteins [16–18]. Both ITCH and TAX1BP1 have been identified as negative regulators of mitochondrial adaptor MAVS, which mediates viral-induced apoptosis [19]. However, no direct link between ITCH and mitochondrial dysfunction has been demonstrated.

Here, we describe a now 20-year-old non-consanguineous White female eventually identified with novel *ITCH* variants who presented with dysmorphic facial features, autoimmune disease including

Table 1
Clinical and Genetic Findings of patients with ITCH deficiency.

	Lohr et al. % of patients affected	Brittain et al.	Kleine-Eggebrecht et al.	Patel et al.	Wolfe Heiman et al.
Current age or age at death	0.6–23 years (10 total patients)	23 years	5 years	18 years	20 years
Living at time of publication	70% living	Yes	No	Yes	Yes
Gender	70% male, 30% female	Female	Female	Male	Female
Ethnicity	Old Order Amish	Caucasian, British and Anglo-Irish heritage	Black, no other information was provided		Caucasian, Polish, German and Slovak heritage
Consanguineous parents	Yes	No	Yes	No	No
Variant (s) (GenBank:NM_031483.7) or (GenBank:NM_001257137)[#]	Homozygous (c.394dupA; p.Ile132Asnfs*9) NM_031483.7	(c.603delA; p.Leu202Serfs*63) and (c.2005_2008delGAAA; p.Glu669Phefs*2) NM_031483.7	Homozygous c.1570-1G > A NM_031483.7	(c.337 + 2 T > C) and (c.772C > T; p.Arg258*) NM_001257137[#]	(c.599dupC; p.Ser201Ilefs*8) and Deletion of exons 24 and 25 NM_031483.7
Hepatomegaly/Splenomegaly	90%	−	+	−	−
failure to thrive	100%	+	?	+	+
Developmental delay	100%	+	+	+	+
Dysmorphic features	100%	+	+	+	+
Scoliosis	0%	−	−	?	+
GERD/Gastroparesis	0%	−	−	−	+
Lung disease	90%	+	+	+	+
Relative macrocephaly	90%	+	+	+	+
Hypotonia	60%	−	+	+	−
Autoimmune disease	60%	−	+	+	+
− Hypothyroidism	40%	−	+	−	−
− Psoriasis	0%	−	−	+	+
− Polymyositis	0%	−	−	−	+
− Hepatitis	30%	−	+	+	+
− Enteropathy	20%	−	+	+	−
− Diabetes mellitus	10%	−	+	+	−
Pancytopenia	0%	−	+	−	−
Liver cirrhosis w/ acute Liver failure	0%	−	+	−	−
Hematopoietic cell transplantation	No	No	No	Yes	No (Planned)

polymyositis, enteropathy, arthritis, psoriasis, hepatitis, and respiratory insufficiency. She also had a history of multiple hospitalizations for infections. Interestingly, the patient initially was evaluated for a mitochondrial respiratory chain disorder at age 5 years, with a muscle biopsy showing 57% of expected mitochondrial DNA copy number but no change in the mitochondrial morphology. Here, we report characterization of cellular mitochondrial bioenergetic function in patient derived fibroblasts to explore the potential role of ITCH in energy metabolism.

2. Materials and methods

2.1. Study design

2.1.1. Consent

This was a single patient study designed to examine functional studies in patient fibroblasts. Informed consent was obtained and approved for participants including patient and parents in accordance with the University of Pittsburgh IRB approved protocol #PRO11070174. All methods were performed in accordance with the relevant guidelines and regulations outlined by the IRB. Whole exome sequencing on a research basis was offered to the family who agreed to participate in the study.

2.1.2. Case selection

The patient was recruited into this research because genetic testing results identified variants in *ITCH* gene not previously described.

2.1.3. Cell culture

Patient and control fibroblasts were grown in Dulbecco's Modified Eagle Medium (DMEM) containing glucose (4.5 g/L) and supplemented with 10% fetal bovine serum, 2 mM glutamine, 100 IU penicillin, 100 μg/mL streptomycin, and 100 μg/mL normocin (InvivoGen, San Diego, CA, USA) at 37 °C, 5% CO_2. For glucose-free conditions, cells were incubated in the same medium minus glucose. Cells were tested regularly for mycoplasma contamination using a PCR Mycoplasma Detection Kit. Cells were used at passage number < 10.

2.1.4. Western blot analysis

Western blotting of whole cell lysates from patient and control fibroblasts was performed as previously described [20]. Twenty five micrograms of protein were loaded onto a 4–15% gradient precast SDS-PAGE gel (Bio-Rad Laboratories, Hercules, CA). Following electrophoresis separated proteins were transferred onto a nitrocellulose membrane. Primary antibodies included anti-ITCH (1;1000, BD Transduction Laboratories, San Jose, CA, #611198), Anti-VLCAD (1:1000, antigen produced by the Vockley Lab, UPMC Children's Hospital of Pittsburgh and antibody generated by Cocalico Biologics, Stevens, PA), Anti-TFP α/β (1:2000, produced by the Vockley Lab), anti-Ubiquitin (1:1000, Abcam, Cambridge, MA, #ab19247), and anti-TXNIP (1:500, Abcam, #ab188865). Blots were incubated with HRP conjugated secondary antibodies. Primary purified mouse anti-GAPDH monoclonal antibody (1,25,000, Abcam, #ab8245) was used as a loading control (Supplemental Table S1). All western blot studies were performed more than once from different celluar lysates (technical replicates).

2.1.5. Measurement of mitochondrial respiration

Cellular oxygen consumption in patient and control fibroblasts was measured with a Seahorse XFe96 Extracellular Flux Analyzer (Agilent, Santa Clara, CA) as previously described using the Seahorse XF Cell Mito Stress Test Kit [21]. Briefly, cells were seeded in 96-well Seahorse tissue culture microplates pre-coated with poly-D-lysine in 8 replicates at a density of 40,000 cells/well 48 h prior to the assay. The cells then were allowed to rest at room temperature for 1 h to prevent edging effects and moved to a 37 °C incubator with 5% CO_2, 95% humidity. Mitochondria functional metric determination successively applied oligomycin, carbonyl cyanide 4-(trifluoromethoxy) phenylhydrazone (FCCP), and Rotenone/antimycin A. OCR data was normalized to protein and reported as pmol/min/μg.

2.1.6. Measurement of ATP production

Total cellular ATP content was determined using the ATPlite™ bioluminescence assay according to the manufacturer's instructions (Supplementary table S2; PerkinElmer Inc. Waltham, MA). Briefly, the day before assay, approximately 10,000 cells/well were seeded in 4 replicates in 96-well plates. The luminescence was measured in a SpectraMax® i3x Platform multi-mode microplate reader system (Molecular Devices, LLC, Sunnyvale, CA). Data are reported in μmol and was normalized to protein and reported as μmol/μg/μL of protein. ATP production rate was obtained using the Seahorse XF Real-Time ATP Rate Assay Kit on a Seahorse XFe96 Extracellular Flux Analyzer (Agilent, Santa Clara, CA). Cells were seeded in 96-well Seahorse tissue culture microplates pre-coated with poly-D-lysine at a density of 60,000 cells/well the day of the assay. The cells were incubated at 37 °C for 1 h with assay buffer that included XF-DMEM media with XF glucose (10 mM), XF L-glutamine (2 mM), XF Na pyruvate (1 mM), and carnitine (0.5 mM). Assessment successively applied oligomycin and Rotenone/antimycin A to determine the ATP production rate from mitochondrial respiration and glycolysis, respectively (Supplemental table S2).

2.1.7. Measurement of superoxide production and mitochondrial mass

Confluent flasks of patient cell lines were incubated for 24 h in either complete or glucose-free DMEM. Four replicates of cell suspension containing 300,000 cells/mL were incubated for 20 min at 37 °C with 5 μM MitoSOX Red (Invitrogen, Grand Island, NY) and 150 nM Mitotracker Green (Invitrogen, Grand Island, NY). After incubation, 50,000 cells were analyzed per cell line in a Becton Dickinson FACSAria II flow cytometer (BD Biosciences, San Jose, CA).

2.1.8. Fatty acid oxidation (FAO) flux assay

Patient and control cells were seeded (350,000 cells/well) onto Corning brand 6-well plates with a seeding density of 350,000 cells per well in triplicates for the assay and duplicates to determine protein concentration, and incubated for 24 h at 37 °C. The plates were then incubated for 2 h in a mixture of glucose-free media supplemented with L-carnitine and 100 μM tritiated [9,10-^{3}H]-oleate conjugated to fatty acid-free albumin, as previously described [22,23]. Protein concentration plates were incubated with mixture of glucose-free media supplemented with L-carnitine only. The reaction mixture was quenched with water, transferred to AG 1-X8 Resin column (Bio-Rad Laboratories), and eluted into scintillation vials. Ten milliliters of scintillation fluid were added to each vial and allowed to incubate at room temperature overnight before counting on a Beckman Coulter LS 6500 MultiPurpose Scintillation Counter (Brea, CA). Data was normalized to the protein concentration. The oxidation rates were expressed as pmol tritium released/h/mg protein.

2.1.9. Cellular immunofluorescence assay

Patient and control fibroblasts were seeded in triplicates on tissue culture-treated glass coverslips at a density of 25,000 cells per coverslip and allowed to grow overnight at 37 °C in 5% CO_2, 95% humidity. Cells were fixed, permeabilized, and blocked as previously described [24]. For ITCH co-localization studies, primary antibodies used include anti-ITCH (1:50, BD Transduction Laboratories, San Jose, CA, # 611198), and anti-ubiquitin (1:50, abcam ab19247). Primary antibody incubation was followed by incubation in an appropriate Alexa Fluor secondary antibody (Invitrogen, Waltham, MA,1:1000) for 1 h at room temperature. DAPI was used for visualization of nuclei. Coverslips were then mounted and imaged on a Zeiss LSM 710 Confocal microscope (ZEISS, White Plains, NY) at 63× magnification.

2.1.10. Cellular apoptosis assay

Apoptosis of patient and control fibroblasts was detected using the In Situ Cell Death Detection Kit, TMR red (Roche Applied Science, Penzberg, Germany) according to the manufacturer's instructions. The day before the assay, 30,000 cells/250 μL were seeded per well in duplicates in a 12 well plate on a tissue culture treated glass coverslips in complete DMEM. The samples were left to incubate at 37 °C in a 5% CO_2, 95% humidity incubator for 45 min and 750 μL of complete DMEM was added to each of the wells. The samples were then incubated overnight at 37 °C in a 5% CO_2, 95% humidity. Samples were then fixed with 4% paraformaldehyde for 15 min at room temperature and permeabilized with Triton X-100 (in 0.1% PBS) with 3 washes of 1× PBS. One sample per cell line was incubated with DNase I for 10 min as a positive control. Next 150 μL of TUNEL reaction mixture (In Situ Cell Death Detection Kit, TMR red; TUNEL; Roche Applied Science, Penzberg, Germany) was added to samples and the positive control. Label solution (300 μL) was added to the negative controls. Samples were incubated for 60 min in the dark, rocking every 5 min, then 300 μL of Phalloidins label F-actin (BioLegend, San Diego, CA; 1:1000) was added and incubated for 25 min, then ~ one minute with 1 μL/mL Hoescht-Blue stain to visualize nuclei. Samples were covered with aqua-polymount and imaged on a Zeiss LSM 710 Confocal microscope at 40× magnification.

2.2. Statistics

Statistical significance was assessed with the unpaired Student's *t*-test using GraphPad Prism version 8.00 for Mac, GraphPad Software (La Jolla, California, USA, www.graphpad.com). A *p*-value <0.05 was considered significant. *p* value: **** <0.0001; *** <0.001; ** <0.01; * < 0.05; ns > 0.05.

3. Results

3.1. Case description

A now 20-year-old Caucasian non-consanguineous female originally presented with history of intrauterine growth retardation, and bilaterally dislocated hips present at birth. She was well until approximately 3 months of life when she was admitted for pneumonia that required mechanical ventilation. At 5 months of age, she was noted to have short limbs with relative macrocephaly and was diagnosed clinically with skeletal dysplasia. Her weight at 5 months of age was 3.9 kg and height was 52 cm (both <3rd centile) with head circumference at 42 cm (~50% centile). She exhibited gross motor and language delays, and dysmorphic features including flat face with mid-facial hypoplasia, bitemporal narrowing, shallow orbits, down slanting palpebral fissures, low set and posteriorly rotated ears, short nose with anteverted nostrils and micrognathia. Short limbs were associated with remarkable muscle wasting on upper and lower extremities (Fig. 1). She was hospitalized frequently beginning at age 3 months with multiple infections, recurrent episodes of polymyositis with muscular weakness, episodic mild elevation of liver transaminases, and respiratory insufficiency with tracheomalacia requiring tracheostomy and chronic mechanical ventilation at 9 months of age. She also had history of GI dysfunction requiring G-tube placement at age 7 months and hydrocephalus requiring ventriculoperitoneal shunt placement at age 20 months.

At age 7 years, she was found to have IgA deficiency, borderline normal IgG levels, and rapidly waning specific antibody responses to

Fig. 1. Clinical features of patient with ITCH deficiency at different ages.
(A) 6 month old with failure to thrive, (B) Patient at 10 years of age with dysmorphic facial features,
(C&D) short limbs and joint deformity with arthritis and muscle wasting. (*E*-I) psoriasis in different areas including guttate pattern in lower extremities (E), scalp (F), fingernails (G), toenails (H) and G-tube site area (I).

Strep. pneumoniae pneumonia. She has been treated with supplemental IgG for the past several years. Bone changes of osteoporosis with pathologic fractures secondary to prolonged steroid use to control inflammatory pulmonary and muscle disease, and possible skeletal dysplasia with markedly delayed bone age, were noted beginning at 5 years of age. Autoimmune findings of psoriasis concentrated at fingers, toes and scalp developed by age 10 years, with initial response to TNF-α inhibitors, but later becoming more aggressive affecting finger and toenail growth, requiring the IL-12/Il-23 inhibitor, stekinemab. Despite daily chronic corticosteroids of 0.5 mg/kg and multiple immunosuppressive agents, she developed autoimmune involvement of the GI tract and liver at the age of 18 years with biopsies of both revealing lymphocytic infiltrate. Sirolimus was initiated (in addition to ongoing Abatacept, Ustekinemab and corticosteroids), and she responded with dramatic improvement in diarrhea, liver enzymes and the repeat endoscopic biopsies of bowel showed decreased inflammation. More recently, she has developed bilateral recurrent Sjogren's like parotiditis at the age of 19 years old. She continues to have arthritis requiring arthrocentesis with drainage and corticosteroid injection of her knees every 6 months. In summary, she has 7 biopsy-proven lymphocytic infiltrates in organs with an autoimmune phenotype and has been treated with multiple concurrent immunosuppressive medications with limited effect, but increasingly apparent that an allogenic stem cell transplant is the next clinical treatment plan.

Metabolic testing including plasma amino acids, acylcarnitine profile, lactate, and urine organic acids were normal.

3.2. Pathology

Liver histology from a biopsy performed at six years of age showed a pattern of centrilobular hepatitis with giant cell transformation (Fig. 2A & 2B). Ultrastructural analysis by electron microscopy revealed elongated, giant, and curved mitochondria in hepatocytes with greater than usual pleomorphism (Fig. 2C-2F). Nodular aggregates of mature collagen were also noted between hepatocytes. These findings were indicative, but not diagnostic of mitochondrial involvement. A muscle biopsy prepared for electron microscopy revealed no ultrastructural abnormalities. When the muscle sample underwent analysis of the electron transport chain., the findings were suggestive of defects in complexes I and II, but activity in complex III was normal. Additional studies showed mitochondrial DNA copy number in muscle was 57% compared to controls. Molecular testing for mitochondrial deletion and duplication was normal (Baylor Medical Genetics Laboratory, Houston, TX).

3.3. Genetic analysis

Whole exome sequencing was performed on a clinical basis and identified a heterozygous variant in the *ITCH* gene. (c.599dupC; p. Ser201Ilefs*8) (GenBank: NM_031483.7) that was maternally inherited. Deletion/duplication studies performed using bi-directional sequencing in a commercial lab identified a de novo deletion of exons 24 and 25 on the second *ITCH* allele (GenBank: NM_031483.7).

3.4. Decreased ubiquitination in ITCH deficient cells

Cellular ITCH protein was detected by western blot analysis from whole cell lysate of control fibroblasts but was absent in lysates from patient derived cells (Fig. 3A). Given the function of ITCH as a ubiquitin ligase, total ubiquitinated proteins were visualized using a ubiquitin specific antibody on western blots, which showed a decrease in patient derived fibroblast lysate compared to control (Fig. 3B). The reduction in ITCH protein and partial reduction in ubiquitinated protein were mirrored by immunofluorescent staining of fibroblasts (Fig. 3C).

3.5. Mitochondria in ITCH deficient cells have dysfunctional bioenergetics

Because of the patient's clinical findings (multi-organ involvement and decreased mitochondrial copy number on muscle biopsy) suggestive of cellular energy deficit, cellular bioenergetics were examined in

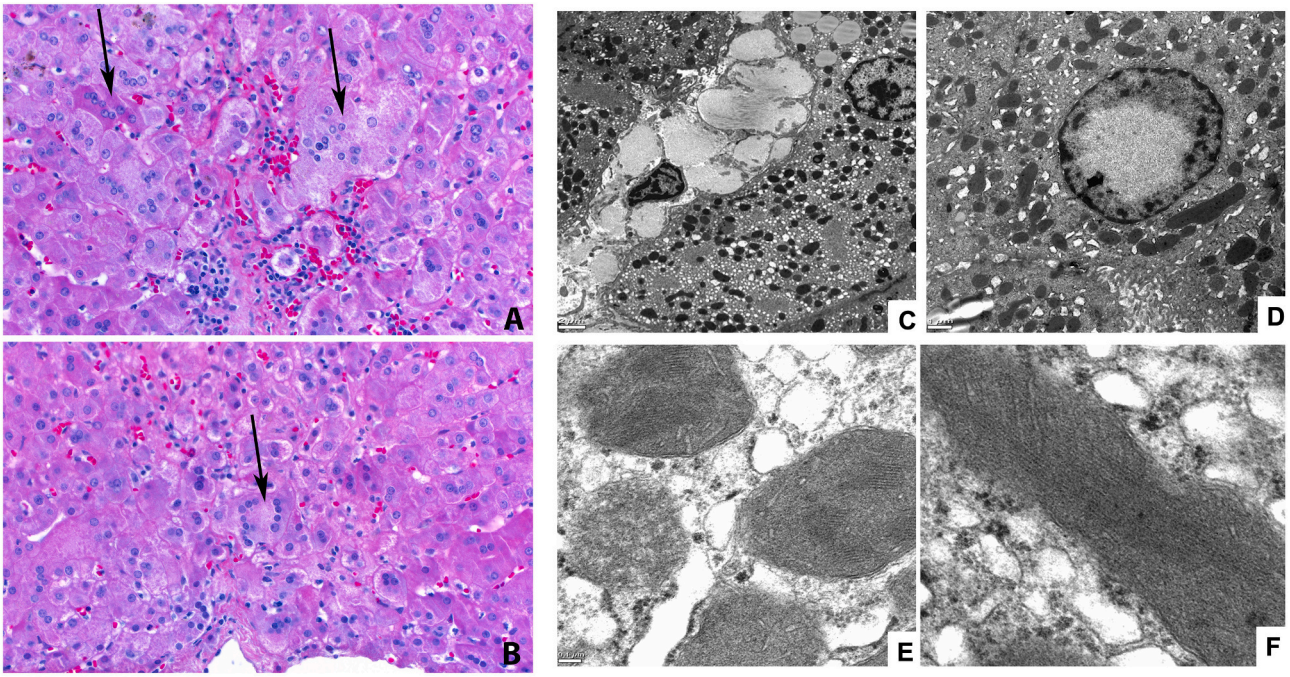

Fig. 2. Histological and ultrastructural analysis of liver tissue from patient with ITCH deficiency.
(A&B) Liver biopsy shows a mild inflammatory infiltrate associated with large and multinucleated hepatocytes, characteristic of hepatocellular giant cell transformation (arrows).
(C—F) Ultrastructural analysis of the liver shows relatively denser mitochondria, with a darker appearance. Some of the mitochondria are elongated and curved (D). At higher magnifications, their cristae are irregular and relatively compressed, as packed in compact clusters.

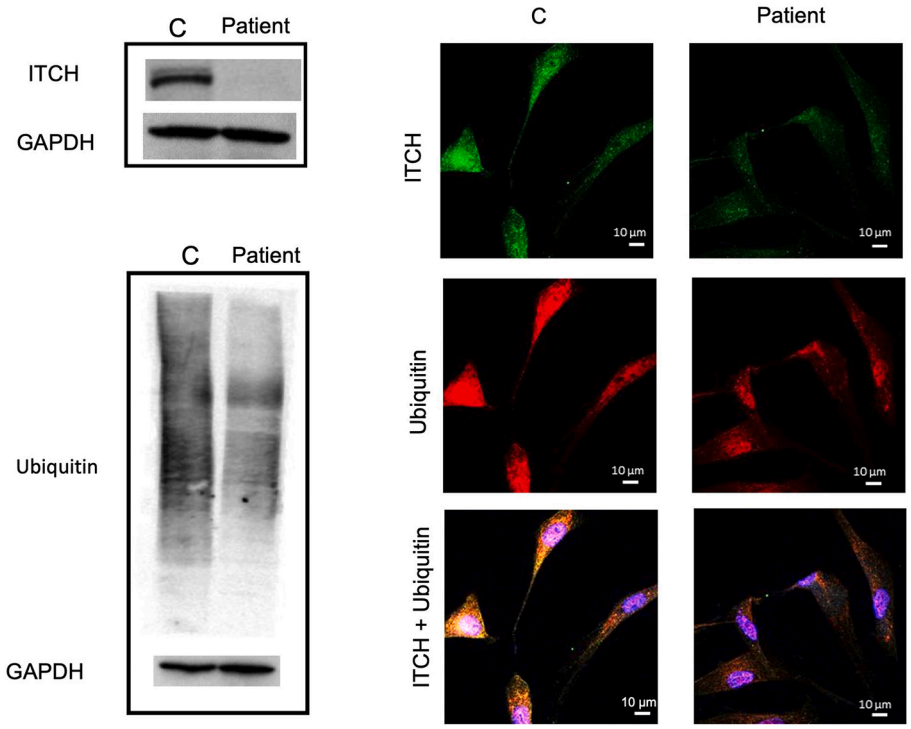

Fig. 3. ITCH and Ubiquitin proteins in control and patient cells.
(A) Whole cell extracts from patient derived and control (C) fibroblasts were analyzed with SDS-PAGE/western blotting and visualized with antisera to ITCH and ubiquitin. GAPDH served as a loading control. Twenty-five μg of protein were loaded in each well. Cropped images shown in this figure; full blots are presented in Supplemental Figs. S1 and S2. (B) Whole cell extracts from patient derived and control fibroblasts were analyzed with SDS-PAGE/western blotting and visualized with antisera to ubiquitin. GAPDH served as a loading control. Twenty-five μg of protein were loaded in each well. (C) Immunofluorescence imaging of patient derived and control cells with fluorescently labeled antibodies to ITCH (green) and ubiquitin (red). The merged image shows co-localization of ITCH with ubiquitin as yellow/orange.

patient derived fibroblasts. The ITCH patient derived cell line demonstrated significant reduction of flux through mitochondrial fatty acid oxidation compared to control fibroblasts measured with tritiated oleate (C18:1) as substrate (Fig. 4A). This correlated with a decrease in the mitochondrial fatty acid oxidation proteins including very long chain acyl-CoA dehydrogenase (VLCAD) and the α-subunit of the mitochondrial trifunctional protein (TFP) in patient derived fibroblasts compared to controls, while the β-subunit of TFP was unchanged (Fig. 4B).

Net cellular ATP content was significantly decreased in the patient fibroblasts compared to controls, regardless of the presence or absence of glucose in the culture media (Fig. 4C). Additionally, the rate of ATP production in patient fibroblasts was decreased compared to controls when cultured in glucose (Fig. 4D). Both glycolytic and mitochondrial ATP production were decreased in patient fibroblasts compared to controls. Mitochondrial respiration measured as oxygen consumption rate (OCR) with a Seahorse Bioanalyzer was significantly decreased for basal respiration, maximal respiration, and spare respiratory capacity in patient fibroblasts compared to controls (Fig. 4E). In total, these results are consistent with global energy imbalance in patient cells.

3.6. *Superoxide production, mitochondrial morphology and apoptosis*

Given the findings of mitochondrial energy production impairment, we next examined several other markers of mitochondrial dysfunction. Superoxide levels in patient fibroblasts was equivalent to controls in the presence of glucose, but were increased compared to controls when grown without glucose (forcing an increased reliance on oxidative phosphorylation; Fig. 5A). TXNIP, a negative regulator of thioredoxin, which is key in ROS regulation, was increased in patient derived fibroblasts relative to control, suggesting it is not being ubiquitinated by ITCH protein due to its deficiency in patient derived fibroblasts (Fig. 5B). The decreased ITCH leads to increase TXNIP, leading to decrease thioredoxin level and therefore contributing to the increase in ROS.

Immunofluorescence due to TMR Red staining, a marker of DNA breaks indicative of the early stage of apoptosis, was present in nuclear segments of patient derived fibroblasts when exposed to hydrogen peroxide. In contrast, no TMR red staining was visualized in control fibroblasts exposed to hydrogen peroxide (Fig. 5C). Complete TMR red immunofluorescence staining results, including positive and negative controls, are included in Supplementary Fig. S4.

4. Discussion

Protein degradation occurs in large part through the ubiquitin-proteasome system (UPS), though certain proteins undergo proteolysis in the lysosomes. The UPS involves the post-translational ubiquitination of proteins as a tag for protein degradation or modification. Ubiquitination occurs in three steps starting with activation of ubiquitin by activating enzymes (E1), followed by transfer of activated ubiquitin to the substrate protein using ubiquitin conjugases (E2), and finally conjugation of the ubiquitin to target proteins by ubiquitin (E3) ligase proteins. There are hundreds of different (E3) ligases, including ITCH, each one recognizing a specific set of proteins to be targeted for degradation/modification by the proteasomal system [25]. Ubiquitination occurs in both the cytosol and the mitochondria [26–28]. The exact number of mitochondrial proteins that are regulated with ubiquitination is not known; however, several proteomic studies report a range from ~25% to ~60% of mitochondrial proteins [29–31]. Additionally, the rate of ubiquitination and protein targets vary depending on the tissue [32]. Though ITCH deficiency has not previously been connected to mitophagy, multiple other E3 ubiquitin ligases have been implicated as mediators of mitophagy, including Mfn1/Mfn2 ubiquitination in the PINK1-Parkin and MARCH5/MITOL signaling axes, respectively [33–35].

In this study, we have identified a novel frameshift variant and novel deletion in the *ITCH* gene in a non-consanguineous Caucasian patient, leading to complete loss of ITCH protein in patient derived fibroblasts. Consistent with the know function of ITCH, patient derived fibroblasts exhibited decreased ubiquitinated proteins compared to control cells.

Further, we have directly demonstrated mitochondrial energy dysfunction in patient derived ITCH deficient fibroblasts, including reduced oxygen consumption (OCR), flux through fatty acid oxidation, and a decrease in cellular ATP production. Additionally, expression of

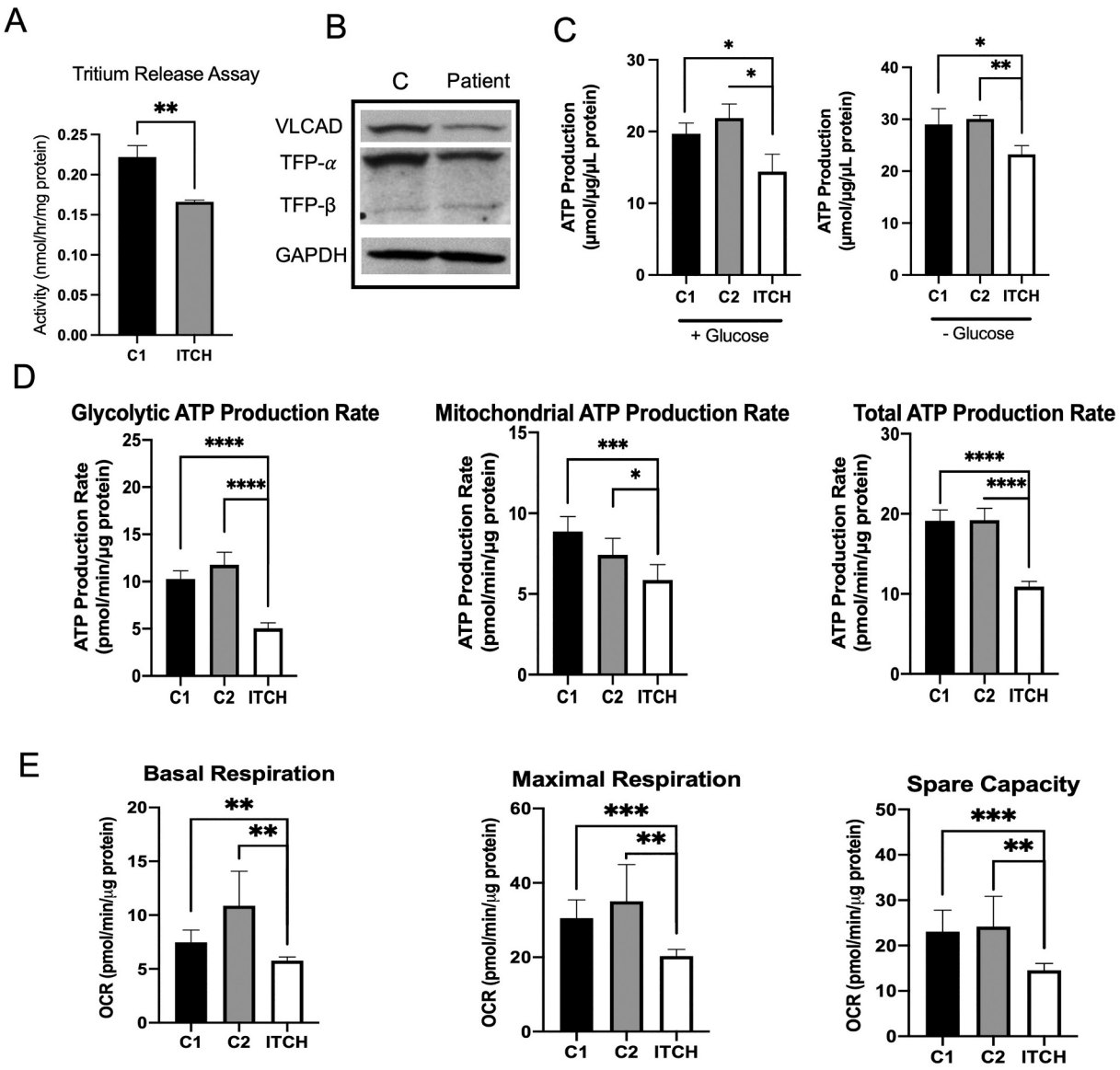

Fig. 4. VLCAD and TFP expression and activity, ATP production and mitochondrial respiration in patient derived and control (C) fibroblasts.
(A) Flux through fatty acid oxidation was measured by release of radiolabeled water from tritiated oleate. Flux was reduced in patient cells compared to control cells. (B) Whole cell extracts from patient derived and control fibroblasts were analyzed with SDS-PAGE/western blotting and visualized with antisera to VLCAD, and TFP alpha and beta subunits. Twenty-five μg protein were loaded in each well, and GAPDH expression served as a loading control. Cropped images are shown; full blots are presented in Supplemental Fig. S3. (C) Net ATP levels were measured in patient derived and control fibroblasts with the ATPlite™ bioluminescence assay kit. (D) The rate of ATP production in patient derived fibroblasts and control cell lines. Glycolytic, mitochondrial, and total ATP production rates are shown. (E) Mitochondrial oxygen consumption was measured in patient derived and two control fibroblasts (C1 and C2). Basal respiration, maximal respiration, and spare capacity are shown. Spare capacity was calculated by subtracting maximal respiration from basal respiration. Statistical analysis was with an unpaired, student's *t*-tests. For experiments with two control groups, separate t-tests were conducted between each control and the patient group. *p* value: **** $\leq$ 0.0001; *** $\leq$ 0.001; ** $\leq$ 0.01; * $\leq$ 0.05; ns $>$ 0.05.

TFP α-subunit, and VLCAD were diminished in patient fibroblasts, supporting the impairment of these pathways by ITCH deficiency.

Notably, patient fibroblasts showed increased mitochondrial superoxide (reactive oxygen species; ROS) production compared to control cells only when grown without glucose, suggesting increased mitochondrial stress compared to cells with active glycolysis (i.e., grown in the presence of glucose). ITCH degrades TXNIP, a regulator of antioxidant thioredoxin that has an anti-apoptotic ROS scavenging activity [7,9,36]. Interestingly, patient fibroblasts had a higher level of TXNIP than control cells, presumably allowing for greater inhibition of thioredoxin and further increasing ROS concentrations in patient cells. Additionally, ITCH deficient fibroblasts had a lower threshold for activation of apoptosis. Together, these results suggest multiple mechanisms that contribute to the oxidative stress in ITCH deficiency, highlighting the need for further disease mechanism studies.

In summary, this study presents a patient with ITCH deficiency with global mitochondrial dysfunction, reduced mitochondrial energy metabolism, increased oxidative stress and apoptosis, and alterations in mitochondrial morphology in patient derived fibroblasts, suggesting new options for therapy for patients with ITCH deficiency. Correlation between ITCH and mitochondrial function offers new potential into the primary cellular role of ITCH and possible explanation for the severe phenotype, the abnormal response to immunosuppression and development of new autoimmune disease in this patient every few years. Additional studies are needed to explore in further details the mitochondrial dynamics under different conditions including stressors.

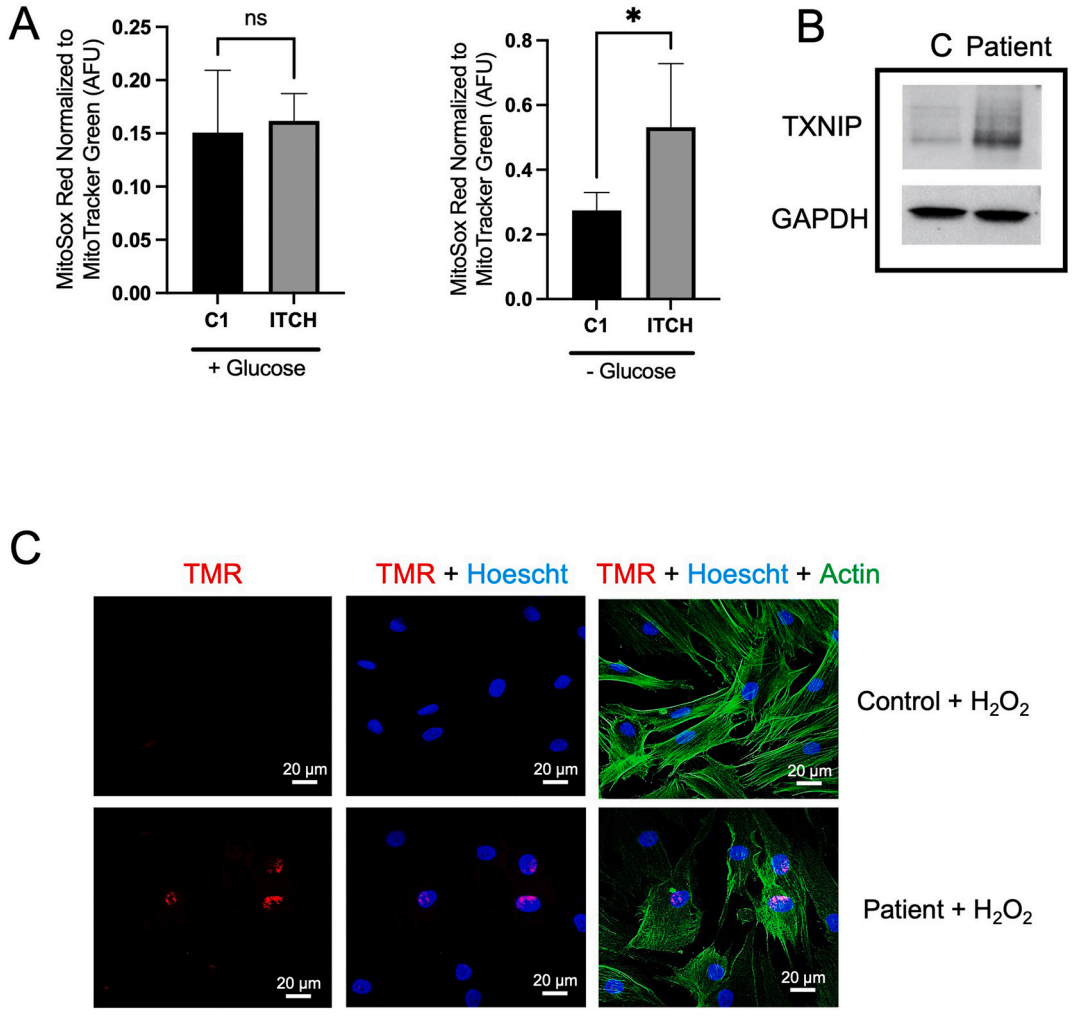

Fig. 5. Measurement of mitochondrial superoxide levels, mitochondrial morphology, and apoptosis in patient derived and control (C) fibroblasts.
(A) Mitochondrial superoxide production was measured in patient derived and control fibroblasts with MitoSox Red and normalized to mitochondrial mass as measured with MitoTracker Green and quantitated by fluorescent cell sorting. Cells were grown in the presence (left panel) or absence (right panel) of glucose. (B) Whole cell extracts from patient derived and control fibroblasts were analyzed by SDS-PAGE/western blotting and visualized with antiserum to TXNIP. GAPDH was used as a loading control. Twenty-five μg protein were loaded in each well. Cropped images are shown; full blots are presented in Supplementary Fig. S4. (C) TUNEL assay of patient and control fibroblasts using TMR red stain (red) and fluorescent-labeled actin (green) antibodies. Nuclei were stained with Hoescht-Blue. Complete images including positive and negative controls are included in Supplemental Figs. S5.1 and S5.2. p value: **** $\leq$ 0.0001; *** $\leq$ 0.001; ** $\leq$ 0.01; * $\leq$ 0.05; ns $>$ 0.05.

Data availability

All materials used in this study are commercially available. All data are available upon request as mandated by NIH guidelines.

Author contributions

RW and PH performed the majority of experiments and drafted the manuscript. RW, PH and LGG developed the experimental design with contribution from AWM and JV. OD performed the fatty acid oxidation (FAO) flux assay. AK performed the immunofluorescent studies. AP and BS assisted with several laboratory studies. MG arranged for the molecular testing on the patient and performed genetic counseling as well as assisted with the clinical summary of the patient. SFD performed the metabolic testing on the patient blood samples, provided the skin fibroblast of the patient. MRM contributed the pathology images and interpretation. KT assisted with the clinical summary of the patient and in the clinical management of the patient. LGG provided clinical summary for the patient and follows patient clinically in the medical genetics' clinic. LGG and JV oversaw the work and reviewed the manuscript. All authors reviewed the manuscript.

Author disclosures

The authors have no competing interests to declare.

Funding

LGG is funded in part by the National Human Genome Research Institute (NHGRI) grant #K08 HG010490, a component of the National Institutes of Health (NIH). The contents of this manuscript are solely the responsibility of the authors and do not necessarily represent the official view of NHGRI/NIH.

Data availability

Data will be made available on request.

Acknowledgements

The authors are grateful to the patient and her family who agreed to participate in this research study. This project was performed in collaboration with the University of Pittsburgh Rangos Metabolic Core Seahorse® Analyzer service, with technical support from Dr. Clinton Van't Land. This project was also performed in collaboration with the University of Pittsburgh Center for Biologic Imaging.

Appendix A. Supplementary data

Supplementary data to this article can be found online at https://doi.org/10.1016/j.ymgmr.2022.100932.

References

[1] A. Hershko, The ubiquitin system for protein degradation and some of its roles in the control of the cell division cycle, Cell Death Differ. 12 (9) (2005) 1191–1197.
[2] A. Ciechanover, Intracellular protein degradation: from a vague idea thru the lysosome and the ubiquitin-proteasome system and onto human diseases and drug targeting, Cell Death Differ. 12 (9) (2005) 1178–1190.
[3] C.M. Hustad, W.L. Perry, L.D. Siracusa, C. Rasberry, L. Cobb, B.M. Cattanach, R. Kovatch, N.G. Copeland, N.A. Jenkins, Molecular genetic characterization of six recessive viable alleles of the mouse agouti locus, Genetics 140 (1) (1995) 255–265.
[4] L.E. Matesic, N.G. Copeland, N.A. Jenkins, Itchy mice: the identification of a new pathway for the development of autoimmunity, Curr. Top. Microbiol. Immunol. 321 (2008) 185–200.
[5] V. Parravicini, et al., Itch−/− alphabeta and gammadelta T cells independently contribute to autoimmunity in itchy mice, Blood 111 (8) (2008) 4273–7282.
[6] H.L. Mentrup, et al., The ubiquitin ligase ITCH coordinates small intestinal epithelial homeostasis by modulating cell proliferation, differentiation, and migration, Differentiation 99 (2018) 51–61.
[7] P. Zhang, et al., The ubiquitin ligase itch regulates apoptosis by targeting thioredoxin-interacting protein for ubiquitin-dependent degradation, J. Biol. Chem. 285 (12) (2010) 8869–8879.
[8] L. Jiang, et al., ITCH regulates oxidative stress induced by high glucose through thioredoxin interacting protein in cultured human lens epithelial cells, Mol. Med. Rep. 22 (5) (2020) 4307–4319.
[9] Y. Otaki, et al., HECT-type ubiquitin E3 ligase ITCH interacts with Thioredoxin-interacting protein and ameliorates reactive oxygen species-induced cardiotoxicity, J. Am. Heart Assoc. 5 (1) (2016).
[10] B.A. Azakir, G. Desrochers, A. Angers, The ubiquitin ligase itch mediates the antiapoptotic activity of epidermal growth factor by promoting the ubiquitylation and degradation of the truncated C-terminal portion of bid, FEBS J. 277 (5) (2010) 1319–1330.
[11] M. Rossi, et al., The E3 ubiquitin ligase itch controls the protein stability of p63, Proc. Natl. Acad. Sci. U. S. A. 103 (34) (2006) 12753–12758.
[12] N.J. Lohr, et al., Human ITCH E3 ubiquitin ligase deficiency causes syndromic multisystem autoimmune disease, Am. J. Hum. Genet. 86 (3) (2010) 447–453.
[13] N. Kleine-Eggebrecht, et al., Mutation in ITCH gene can cause syndromic multisystem autoimmune disease with acute liver failure, Pediatrics 143 (2) (2019).
[14] H.K. Brittain, et al., Biallelic human ITCH variants causing a multisystem disease with dysmorphic features: a second report, Am. J. Med. Genet. A 179 (7) (2019) 1346–1350.
[15] T. Patel, et al., Immune dysregulation in human ITCH deficiency successfully treated with hematopoietic cell transplantation, J Allergy Clin Immunol Pract 9 (7) (2021) 2885–2893 e3.
[16] P.E. Bonnen, et al., Mutations in FBXL4 cause mitochondrial encephalopathy and a disorder of mitochondrial DNA maintenance, Am. J. Hum. Genet. 93 (3) (2013) 471–481.
[17] X. Gai, et al., Mutations in FBXL4, encoding a mitochondrial protein, cause early-onset mitochondrial encephalomyopathy, Am. J. Hum. Genet. 93 (3) (2013) 482–495.
[18] M. Huemer, et al., Clinical, morphological, biochemical, imaging and outcome parameters in 21 individuals with mitochondrial maintenance defect related to FBXL4 mutations, J. Inherit. Metab. Dis. 38 (5) (2015) 905–914.
[19] Y.B. Choi, et al., TAX1BP1 restrains virus-induced apoptosis by facilitating itch-mediated degradation of the mitochondrial adaptor MAVS, Mol. Cell. Biol. 37 (1) (2017).
[20] M.B. de Moura, et al., Overexpression of mitochondrial sirtuins alters glycolysis and mitochondrial function in HEK293 cells, PLoS One 9 (8) (2014), e106028.
[21] P. Heiman, et al., Mitochondrial dysfunction associated with TANGO2 deficiency, Sci. Rep. 12 (1) (2022) 3045.
[22] B. Seminotti, et al., Mitochondrial energetics is impaired in very long-chain acyl-CoA dehydrogenase deficiency and can be rescued by treatment with mitochondria-targeted electron scavengers, Hum. Mol. Genet. 28 (6) (2019) 928–941.
[23] E.S. Goetzman, et al., Long-chain acyl-CoA dehydrogenase deficiency as a cause of pulmonary surfactant dysfunction, J. Biol. Chem. 289 (15) (2014) 10668–10679.
[24] M. Schiff, et al., Molecular and cellular pathology of very-long-chain acyl-CoA dehydrogenase deficiency, Mol. Genet. Metab. 109 (1) (2013) 21–27.
[25] J.Z. Roberts, N. Crawford, D.B. Longley, The role of ubiquitination in apoptosis and necroptosis, Cell Death Differ. 29 (2022) 272–284.
[26] J. Lavie, et al., Ubiquitin-dependent degradation of mitochondrial proteins regulates energy metabolism, Cell Rep. 23 (10) (2018) 2852–2863.
[27] S. Gehrke, et al., PINK1 and Parkin control localized translation of respiratory chain component mRNAs on mitochondria outer membrane, Cell Metab. 21 (1) (2015) 95–108.
[28] V.A. Gold, et al., Visualization of cytosolic ribosomes on the surface of mitochondria by electron cryo-tomography, EMBO Rep. 18 (10) (2017) 1786–1800.
[29] N.D. Udeshi, et al., Refined preparation and use of anti-diglycine remnant (K-epsilon-GG) antibody enables routine quantification of 10,000s of ubiquitination sites in single proteomics experiments, Mol. Cell. Proteomics 12 (3) (2013) 825–831.
[30] S.A. Wagner, et al., A proteome-wide, quantitative survey of in vivo ubiquitylation sites reveals widespread regulatory roles, Mol. Cell. Proteomics 10 (10) (2011). M111 013284.
[31] G. Lehmann, R.G. Udasin, A. Ciechanover, On the linkage between the ubiquitin-proteasome system and the mitochondria, Biochem. Biophys. Res. Commun. 473 (1) (2016) 80–86.
[32] S.A. Wagner, et al., Proteomic analyses reveal divergent ubiquitylation site patterns in murine tissues, Mol. Cell. Proteomics 11 (12) (2012) 1578–1585.
[33] E. Ziviani, A.J. Whitworth, How could Parkin-mediated ubiquitination of mitofusin promote mitophagy? Autophagy 6 (5) (2010) 660–662.
[34] R. Yonashiro, et al., A novel mitochondrial ubiquitin ligase plays a critical role in mitochondrial dynamics, EMBO J. 25 (15) (2006) 3618–3626.
[35] S. Pickles, P. Vigie, R.J. Youle, Mitophagy and quality control mechanisms in mitochondrial maintenance, Curr. Biol. 28 (4) (2018) R170–R185.
[36] A.M. Kaimul, et al., Thioredoxin and thioredoxin-binding protein-2 in cancer and metabolic syndrome, Free Radic. Biol. Med. 43 (6) (2007) 861–868.